Chapter 1
From finite to incremental strain: Insights into heterogeneous shear zone evolution

STEFANO VITALE and STEFANO MAZZOLI

Dipartimento di Scienze della Terra, dell'Ambiente e delle Risorse (DiSTAR), Università degli studi di Napoli 'Federico II', Largo San Marcellino 10, 80138, Napoli, Italy

1.1 INTRODUCTION

Heterogeneous ductile shear zones are very common in the Earth's lithosphere and are particularly well exposed in mountain belts (e.g. Iannace and Vitale 2004; Yonkee 2005; Vitale et al. 2007a,b; Okudaira and Beppu 2008; Alsleben et al. 2008; Sarkarinejad et al. 2010; Kuiper et al. 2011; Dasgupta et al. 2012; Zhang et al. 2013; Samani 2013; Mukherjee 2013, 2014; also see Chapter 9), where they provide useful tools for a better understanding of the processes and parameters controlling strain localization, type of deformation, and rock rheology. The occurrence of strain markers such as fossils, ooids and ellipsoidal clasts in sedimentary rocks, or equant minerals, deflected veins and dykes in igneous rocks, allows one to quantify the finite strain by means of various methods (e.g. Dunnet 1969; Fry 1979; Lisle 1985; Erslev 1988; Vitale and Mazzoli 2005, 2010).

Finite strains are all quantities, directly measured or derived, related to the final state of deformation. These finite quantities, such as strain ratio, effective shear strain (*sensu* Fossen and Tikoff 1993), and angle θ' between the shear plane and oblique foliation in heterogeneous ductile shear zones, cannot furnish unequivocal information about the temporal strain evolution (i.e. strain path; Flinn 1962). This is because there are several combinations of deformation types such as simple shear, pure shear and volume change, that can act synchronously or at different times, leading to the same final strain configuration (Tikoff and Fossen 1993; Fossen and Tikoff 1993; Vitale and Mazzoli 2008, 2009; Davis and Titus 2011). Appropriate constraints are needed to obtain a unique solution – or at least reduce the underdetermination. This also implies introducing some assumptions in the definition of the strain model. The strain path may be envisaged as a temporal accumulation of small strain increments, and the final strain arrangement as the total addition (Ramsay 1967). A possible relationship between final strain configuration and temporal evolution (i.e. incremental strains) was suggested by different authors, such as Hull (1988), Mitra (1991) and Means (1995). The latter author envisaged strain softening/hardening as the main rheological control on shear zone evolution: shear zones characterized by a thickness decreasing with time (Type II) result from strain softening, whereas shear zones characterized by increasing thickness (Type I) are produced by strain hardening (Means 1995). Based on this view, each part of a heterogeneous ductile shear zone is the result of a different strain evolution, and taken all together, the various shear zone sectors may be able to record the whole strain history.

During the last few years, several papers dealt with the possibility of calculating the incremental strain knowing the temporal and spatial evolution of the deformation. Provost et al. (2004) reconstruct the deformation history by means of the n times iteration of the transforming equation characterizing the incremental strain, where n is the number of deformation stages. Horsman and Tikoff (2007) focus the opportunity of separating, by previous method, the strain related to the shear zone margins, where according to Ramsay (1980) the deformation is weak, and that associated with the more deformed shear zone sectors. The authors consider heterogeneous shear zones as consisting of sub-zones, each characterized by a roughly homogeneous deformation. Based on their temporal and spatial evolution, shear zones are then classified into three main groups: (i) constant-volume deformation, (ii) localizing, and (iii) delocalizing deformation. In the first case, the shear zone boundaries remain fixed (Type III shear zone of Hull (1988); Mitra (1991); Means (1995)), whereas for the latter two groups the shear zone boundaries migrate with time, leading to decreasing (group ii) or increasing (group iii) thickness of the actively deforming zone (respectively Type II and Type I shear zones of Hull (1988); Mitra (1991); Means (1995).

Following Means (1995), Vitale and Mazzoli (2008) provide a mathematical forward model of strain accumulation within an ideal heterogeneous shear zone by subdividing it into n homogenously deformed layers, each one

Ductile Shear Zones: From Micro- to Macro-scales, First Edition. Edited by Soumyajit Mukherjee and Kieran F. Mulchrone.

bound by shear planes (C-planes: Passchier and Trouw 2005) and characterized by a specific evolution, this being related to that of adjacent layers within the framework of a defined temporal succession. In the case of strain hardening, the strain evolution starts with a homogeneous deformation affecting originally a specific volume of rock (being represented by a single layer in the model). As the original "single layer" is able to accumulate only a specific amount of strain (due to strain hardening), further shearing involves new material located along the shear zone margins (Mazzoli and Di Bucci 2003; Mazzoli et al. 2004), thereby increasing the active shear zone volume (delocalizing zone of Horsman and Tikoff 2007). On the contrary, in the strain softening case, the deformation – originally homogeneous and affecting an ideal "multilayer" – progressively abandons the layers located at the shear zone margins due to easier strain accumulation in the central sector (localizing zone of Horsman and Tikoff 2007). The difference between the approach of Horsman and Tikoff (2007) and that of Vitale and Mazzoli (2008) is that the latter authors relate the temporal and spatial evolution of the shear zone to strain softening/hardening, whereas the former authors avoid any genetic implication.

Building on the results obtained by Vitale and Mazzoli (2008), and following the mathematical approach of Provost et al. (2004) and Horsman and Tikoff (2007), a technique is proposed in this paper, which is able to provide information on the incremental strain path based on measured finite strains. The incremental strain analysis is then applied to a heterogeneous wrench zone characterized by no stretches along the shear direction and no volume change.

1.2 INCREMENTAL STRAIN

To obtain a mathematical relationship between incremental and finite strain, consider the general case of deformation being localized within a heterogeneous ductile shear zone with synchronous deformation in the host rock. The shear zone is composed of n deformed layers, each characterized by homogeneous strain. The strain evolution is illustrated in Fig. 1.1 when strain softens (localizing shear zone) and hardens (delocalizing shear zone), where matrices $\mathbf{B}_i$ and $\mathbf{C}^{\mathbf{fin}}$ represent finite strain within the shear zone and in the host rock in the last configuration, respectively, whereas matrices $\mathbf{A}_i$ and $\mathbf{C}$ are related to incremental strain.

In the case of a localizing shear zone, indicating with $\boldsymbol{B}_i$ the finite strain matrix of the i-th layer in the last configuration (n), the finite strain matrix is related to the incremental matrices by the following relationships (with i ranging between 2 to $n-1$):

$$\begin{aligned}
&\mathbf{B}_1 = \mathbf{C}^{n-1}\mathbf{A}_1 \rightarrow (\mathbf{C}^{n-1})^{-1}\mathbf{B}_1 = (\mathbf{C}^{n-1})^{-1}(\mathbf{C}^{n-1})\mathbf{A}_1 \rightarrow \\
&\quad \mathbf{A}_1 = (\mathbf{C}^{n-1})^{-1}\mathbf{B}_1, \\
&\mathbf{B}_2 = \mathbf{C}^{n-2}\mathbf{A}_2\mathbf{A}_1 \rightarrow \mathbf{B}_2 = \mathbf{C}^{n-2}\mathbf{A}_2(\mathbf{C}^{n-1})^{-1}\mathbf{B}_1 \rightarrow \\
&\quad \mathbf{A}_2 = (\mathbf{C}^{n-2})^{-1}\mathbf{B}_2(\mathbf{B}_1)^{-1}\mathbf{C}^{n-1}, \ldots\ldots \\
&\quad \mathbf{A}_i = (\mathbf{C}^{n-i})^{-1}\mathbf{B}_i(\mathbf{B}_{i-1})^{-1}\mathbf{C}^{n-i+1}.
\end{aligned} \tag{1}$$

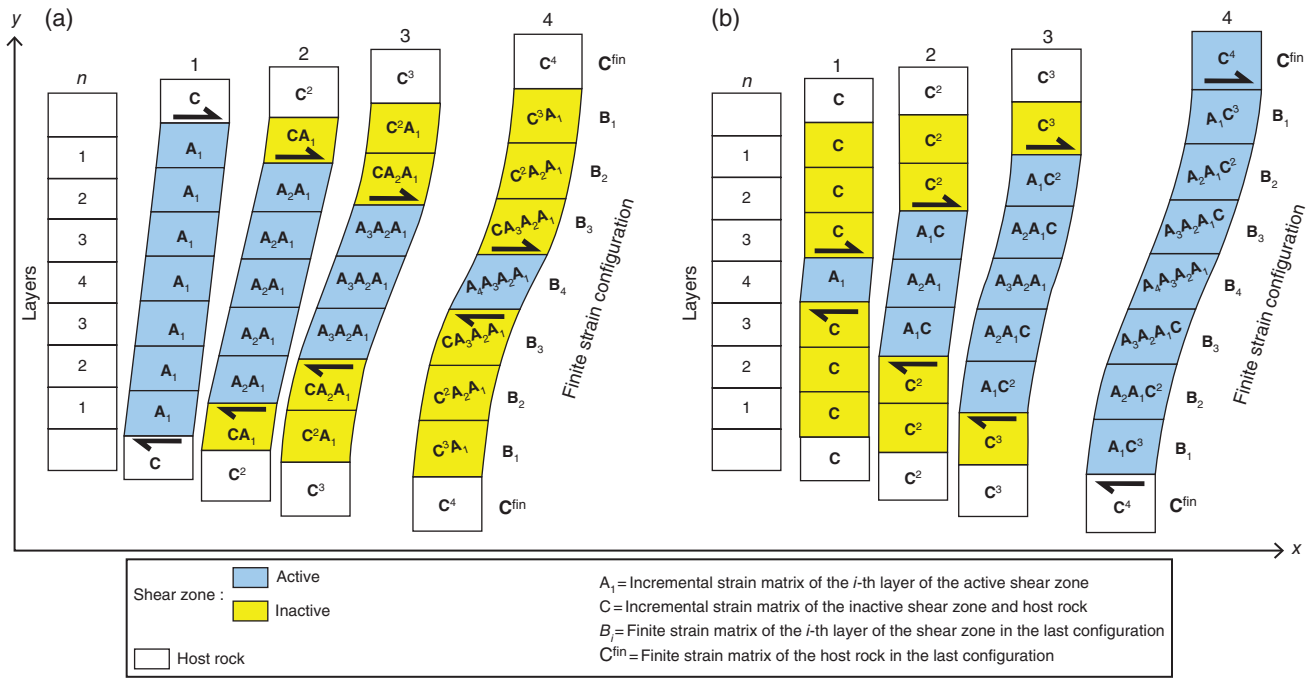

Fig. 1.1. Examples of strain evolution along the *xy* plane of the coordinate reference frame for heterogeneous shear zones consisting of seven homogeneously deformed layers and characterized by transtension in the active shear zone and synchronous pure shear elsewhere. (a) Localizing shear zone. (b) Delocalizing shear zone.

In the case of a delocalizing shear zone the relationship is:

$$\mathbf{A}_i = \mathbf{B}_i \left(\mathbf{C}^{n-i}\right)^{-1} \mathbf{C}^{n-i+1} \left(\mathbf{B}_{i-1}\right)^{-1} = \mathbf{B}_i \mathbf{C} \left(\mathbf{B}_{i-1}\right)^{-1}. \quad (2)$$

1.2.1 Special case of no deformation in the host rock

In the case of $\mathbf{C} = 1$ (identity matrix), i.e. no deformation in the host rock, Equations (1) and (2) are always substituted by the equation:

$$\mathbf{A}_i = \mathbf{B}_i \left(\mathbf{B}_{i-1}\right)^{-1}. \quad (3)$$

In this circumstance, the relationships between incremental and finite strain quantities (stretches and effective shear strains) may be directly obtained by rewriting Equation 3 in an explicit form. Consider a wrench zone in which each *i*-th layer is characterized by finite strain represented by the matrix (Tikoff and Fossen 1993):

$$\mathbf{B}_i = \begin{bmatrix} \left(k_1^{fin}\right)_i & \Gamma_i^{fin} & 0 \\ 0 & \left(k_2^{fin}\right)_i & 0 \\ 0 & 0 & \left(k_3^{fin}\right)_i \end{bmatrix}, \quad (4)$$

where

$$\Gamma_i^{fin} = \gamma_i^{fin} \left(\frac{\left(k_1^{fin}\right)_i - \left(k_2^{fin}\right)_i}{\ln\left(\frac{\left(k_1^{fin}\right)_i}{\left(k_2^{fin}\right)_i} \right)} \right) \quad (5)$$

is the *i*-th finite effective shear strain.

Applying Equation 3 this yields:

$$\mathbf{A}_i = \mathbf{B}_i \mathbf{B}_{i-1}^{-1} = \begin{bmatrix} \frac{\left(k_1^{fin}\right)_i}{\left(k_1^{fin}\right)_{i-1}} & \frac{\Gamma_i^{fin}}{\left(k_2^{fin}\right)_{i-1}} - \frac{\left(k_1^{fin}\right)_i}{\left(k_1^{fin}\right)_{i-1}} \frac{\Gamma_{i-1}^{fin}}{\left(k_2^{fin}\right)_{i-1}} & 0 \\ 0 & \frac{\left(k_2^{fin}\right)_i}{\left(k_2^{fin}\right)_{i-1}} & 0 \\ 0 & 0 & \frac{\left(k_3^{fin}\right)_i}{\left(k_3^{fin}\right)_{i-1}} \end{bmatrix}, \quad (6)$$

where $\mathbf{A}_i$ is the incremental matrix referred to the *i*-th step.

The relationships between incremental and finite quantities are obtained:

$$\left(k_1^{incr}\right)_i = \frac{\left(k_1^{fin}\right)_i}{\left(k_1^{fin}\right)_{i-1}}; \left(k_2^{incr}\right)_i = \frac{\left(k_2^{fin}\right)_i}{\left(k_2^{fin}\right)_{i-1}}; \left(k_3^{incr}\right)_i = \frac{\left(k_3^{fin}\right)_i}{\left(k_3^{fin}\right)_{i-1}} \quad (7)$$

and

$$\Gamma_i^{incr} = \frac{\Gamma_i^{fin}}{\left(k_2^{fin}\right)_{i-1}} - \frac{\left(k_1^{fin}\right)_i}{\left(k_1^{fin}\right)_{i-1}} \frac{\Gamma_{i-1}^{fin}}{\left(k_2^{fin}\right)_{i-1}}. \quad (8)$$

In the case of a transpressional/transtensional wrench zone with $k_1 = 1$ and $k_2 k_3 = 1$, equation (8) becomes:

$$\Gamma_i^{incr} = \frac{\Gamma_i^{fin}}{\left(k_2^{fin}\right)_{i-1}} - \frac{\Gamma_{i-1}^{fin}}{\left(k_2^{fin}\right)_{i-1}} = \left(\Gamma_i^{fin} - \Gamma_{i-1}^{fin}\right)\left(k_3^{fin}\right)_{i-1}. \quad (9)$$

Note that, for a deformation characterized by simple shear only ($k_1 = k_2 = k_3 = 1$), the incremental shear strain corresponds to the finite shear strain increment.

In the case of no synchronous pure shear deformation in the host rock (i.e. $\mathbf{C} = 1$), the final strain configurations of localizing and delocalizing shear zones (Fig. 1.1) are indistinguishable. However, according to Means (1995), useful information may be obtained by the analysis of the shear strain across the shear zone. In the case of strain softening, which is assumed to control the development of localizing shear zones, the finite shear strain profile displays a peaked shape. On the contrary, in the case of strain hardening (i.e. in the case of delocalizing shear zones) the profile is flat-shaped. Therefore an accurate study of the shear strain gradient across the shear zone may effectively unravel the type of rheological behaviour (strain hardening/softening) characterizing the analysed structure.

1.3 FINITE STRAIN

It is generally very difficult to obtain all four parameters of the finite matrix (Equation 4) by analyzing naturally deformed shear zones. However, in some cases, it is possible to determine all derived strain parameters starting from measured ones. Among these, the case of a shear zone characterized by no volume variation and nor stretch along the *x* direction ($k_1 = 1$).

Consider a wrench zone (Fig. 1.2) where each *i*-th layer is characterized by synchronous simple and pure shear represented by the finite strain matrix (in order to simplify the formulae, the label *i* is omitted and all quantities have to be considered as finite values):

$$\mathbf{B} = \begin{bmatrix} 1 & \Gamma & 0 \\ 0 & k_2 & 0 \\ 0 & 0 & k_3 \end{bmatrix}. \quad (10)$$

Generally one can directly measure only the (R, θ') and/or (Γ,θ') values, where R is the aspect ratio of the finite strain ellipse (e.g. Ramsay and Huber 1983) and θ' is the angle between the finite strain ellipsoid XY plane and the shear plane *xy* (e.g. Vitale and Mazzoli 2008, 2010). R and Γ can be obtained using the R_f/ϕ method

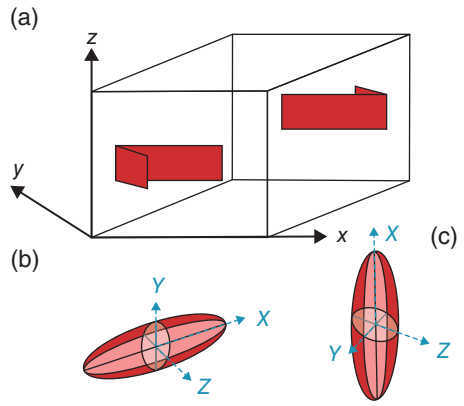

Fig. 1.2. (a) Cartoon showing a homogeneous wrench zone. (b) Finite strain ellipsoid geometry in case the *x*-axis lies in the *xy* plane of the coordinate reference frame. (c) Finite strain ellipsoid geometry in case the *x*-axis is parallel to the *z*-axis of the coordinate reference frame.

(Dunnet 1969) and the cotangent rule (Ramsay and Huber 1983; Vitale and Mazzoli 2010), respectively. Starting from the values of R and θ', let us try to find other strain parameters such as shear strain and stretches. To obtain a relationship between k and Γ, let us calculate the mathematical expression of the principal strain ratios R_{XZ}, R_{YZ} and R_{XY} starting from the magnitudes of the strain ellipsoid axes ($\lambda_{1,2,3}$), corresponding to the eigenvalues of the matrix $\mathbf{BB^T}$ (where $\mathbf{B^T}$ is the transposed matrix of $\mathbf{B}$):

$$\left(\mathbf{BB}^{\mathrm{T}}-\lambda\mathbf{I}\right)\mathbf{e}=\left(\mathbf{BB}^{\mathrm{T}}-\lambda\mathbf{I}\right)\begin{bmatrix}x\\y\\z\end{bmatrix}=\begin{bmatrix}\left(1+\Gamma^2-\lambda\right)x+\Gamma k_3 z\\\left(k_2^2-\lambda\right)y\\\Gamma k_3 x+\left(k_3^2-\lambda\right)z\end{bmatrix}=0, \tag{11}$$

where $\mathbf{e}$ is the eigenvector and $\mathbf{I}$ is the identity matrix.

The solution is:

$$\lambda_{1,2,3}=\begin{cases}k_2^2\\\frac{1}{2}\left(k_3^2+\Gamma^2+1+\sqrt{k_3^4+2k_3^2\Gamma^2-2k_3^2+\Gamma^4+2\Gamma^2+1}\right).\\\frac{1}{2}\left(k_3^2+\Gamma^2+1-\sqrt{k_3^4+2k_3^2\Gamma^2-2k_3^2+\Gamma^4+2\Gamma^2+1}\right)\end{cases} \tag{12}$$

Indicating with λ_1, λ_2 and λ_3 the maximum, intermediate and minimum value, respectively (i.e. $\lambda_1>\lambda_2>\lambda_3$), the strain ratios of the principal finite strain ellipses are:

$$R_{XZ}=\sqrt{\frac{\lambda_1}{\lambda_3}};R_{YZ}=\sqrt{\frac{\lambda_2}{\lambda_3}};R_{XY}=\sqrt{\frac{\lambda_1}{\lambda_2}}. \tag{13}$$

In order to find the angle θ' between the *xz* plane of the reference coordinate system (parallel to the shear plane) and the *XY* plane of the finite strain ellipsoid (parallel to the foliation) from the first equation of the system (Equation 11) and choosing the appropriate value of λ^*, the angle θ' is obtained as follows:

$$-\frac{1+\Gamma^2-\lambda^*}{\Gamma k_3}=\frac{z}{x}=\tan\theta'. \tag{14}$$

The *X*-axis of the strain ellipsoid (the maximum stretching) can lie in the *xz* plane (Fig. 1.2b) or be parallel to the *y*-axis (Fig. 1.2c) of the reference coordinate system. In both cases the value of λ^* in the Equation 14 is

$$\lambda^*=\frac{1}{2}\left(k_3^2+\Gamma^2+1+\sqrt{k_3^4+2k_3^2\Gamma^2-2k_3^2+\Gamma^4+2\Gamma^2+1}\right); \tag{15}$$

substituting the value of λ^* of Equation 15 in the formula (Equation 14), the resulting equation is

$$(\tan\theta')\,k_3\Gamma+\Gamma^2+1-\frac{1}{2}\left(k_3^2+\Gamma^2+1+\sqrt{k_3^4+2k_3^2\Gamma^2-2k_3^2+\Gamma^4+2\Gamma^2+1}\right)=0,$$

which simplifies to

$$(\tan\theta')\,k_3^2-\Gamma\left((\tan\theta')^2-1\right)k_3-(\tan\theta')(\Gamma^2+1)=0. \tag{16}$$

Solving for k_3 yields

$$k_3=\frac{\Gamma(\tan\theta')^2-\Gamma+\sqrt{\Gamma^2(\tan\theta')^4+2\Gamma^2(\tan\theta')^2+\Gamma^2+4(\tan\theta')^2}}{2\tan\theta'} \tag{17}$$

and

$$k_3=\frac{\Gamma(\tan\theta')^2-\Gamma-\sqrt{\Gamma^2(\tan\theta')^4+2\Gamma^2(\tan\theta')^2+\Gamma^2+4(\tan\theta')^2}}{2\tan\theta'}. \tag{18}$$

The solution for k_3 in Equation 18 provides negative values (k_3 must be ≥ 0), and hence has to be eliminated.

In order to find a suitable equation to join with Equation 17 in the variables k_3 and Γ, let us consider the strain ratio relationship

$$R-\sqrt{\frac{k_3^2+\Gamma^2+1+\sqrt{k_3^4+2k_3^2\Gamma^2-2k_3^2+\Gamma^4+2\Gamma^2+1}}{k_3^2+\Gamma^2+1-\sqrt{k_3^4+2k_3^2\Gamma^2-2k_3^2+\Gamma^4+2\Gamma^2+1}}}=0. \tag{19}$$

If the direction of the maximum lengthening (*x*-axis of the strain ellipsoid) lies in the *xy* plane of the reference coordinate system (Fig. 1.2a) than the second value of λ in the Equation 12 is the maximum one and $R = R_{XZ}$, else if the *X*-axis is parallel to the *z*-axis (Fig. 1.2b), the second value of λ is the intermediate one and $R = R_{YZ}$. Solving for k_3 yields

$$k_3 = \frac{\pm\left(-1-R^2\right) \pm \sqrt{1-R^2+R^4-4R^2\Gamma^2}}{2R} \tag{20}$$

In order to obtain real solutions the argument of the square root must be zero or positive, hence

$$1-R^2+R^4-4R^2\Gamma^2 \geq 0,$$

with $R \geq 1$ and $\Gamma \geq 0$. These inequalities hold only when $R \geq \Gamma + \sqrt{\Gamma^2+1}$. Under this condition, the solutions that furnish positive values are

$$k_3 = \frac{1+R^2 \pm \sqrt{1-R^2+R^4-4R^2\Gamma^2}}{2R}. \tag{21}$$

Combining Equations 21 and 17 yields

$$\frac{\Gamma \tan\theta'^2 - \Gamma + \sqrt{\Gamma^2 \tan\theta'^4 + 2\Gamma^2 \tan\theta'^2 + \Gamma^2 + 4\tan\theta'^2}}{2\tan\theta'} = \frac{1+R^2 \pm \sqrt{1-R^2+R^4-4R^2\Gamma^2}}{2R}. \tag{22}$$

Solving for Γ gives the only positive and real solution

$$\Gamma = \frac{R^2-1}{R}\frac{\tan\theta'}{1+\tan\theta'^2}. \tag{23}$$

To find k_3 we can substitute the formula (Equation 23) into Equation 17. Furthermore $k_2 = k_3^{-1}$ and for the others strain quantities, such as shear strain and kinematic vorticity number, we can use the following equations, respectively:

$$\gamma = \frac{\Gamma \log\left(k_3\right)}{\left(1-k_2\right)} \tag{24}$$

and

$$W_k = \frac{\gamma}{\sqrt{2\left(\log\left(k_2\right)^2 + \log\left(k_3\right)^2\right)+\gamma^2}} = \frac{\gamma}{\sqrt{4log\left(k_3\right)^2+\gamma^2}}. \tag{25}$$

Summarizing, in the special case of $k_1 = k_2k_3 = 1$, starting from the strain ratio (R_{XZ} if the strain ellipsoid *X*-axis lies in the *xz* plane, or R_{YZ} if the strain ellipsoid *x*-axis is parallel to the *y*-axis) and the angle θ' that the foliation forms with the shear plane, it is possible to obtain the values of k_3 (and k_2), γ and W_k by means of Equations 16, 23, 24, and 25.

1.4 PRACTICAL APPLICATION OF INCREMENTAL AND FINITE STRAIN ANALYSES

The technique proposed in this study is applied to a heterogeneous ductile wrench zone (Fig. 1.3a), previously analyzed by Vitale and Mazzoli (2010), exposed in a low-strain domain of an elsewhere extensively deformed and mylonitized pre-Alpine intrusive granitoid body included within the amphibolite facies *Zentralgneiss* (Penninic units exposed within the Tauern tectonic window, Eastern Alps; Fig. 1.3c; Mancktelow and Pennacchioni 2005; Pennacchioni and Mancktelow 2007). Shear zone nucleation was controlled by the presence of precursor joints, and occurred by a widespread reactivation process that characterizes solid-state deformation of granitoid plutons also elsewhere (e.g. Pennacchioni 2005; Mazzoli et al. 2009). Wrench zones are characterized by a well-developed foliation and deformed quartz veins that are intersected by the shear zone themselves (Fig. 1.3a). Wrench zones are subvertical and characterized by sub-horizontal slip vectors, and sinistral and dextral sense of shear. Geochemical analyses of major and trace elements of deformed and undeformed rocks (Pennacchioni 2005), indicate no geochemical changes occurred during deformation and hence suggesting that the deformation involved no volume variation (Grant 1986).

1.4.1 Finite strain

The analyzed wrench zone is characterized by localized synchronous simple shear and pure shear. The main finite strain parameters of the shear zone were evaluated by analyzing deformed planar markers (Vitale and Mazzoli 2010). In this case, the shear zone was divided into layers characterized by a roughly homogeneous internal deformation (Fig. 1.3b). For each layer, finite quantities of θ' and Γ were measured and plotted in a scatter diagram (Fig. 1.4). The latter also includes a k_2–γ grid that was constructed considering the known conditions of no volume change ($\Delta = 0$) and assuming $k_1 = 1$ (i.e. transpressional/transtensional deformation *sensu* Sanderson and Marchini 1984) by varying the stretch k_2 and the shear strain γ in the equations:

$$\Gamma = \frac{\gamma\left(1-k_2\right)}{\log\left(k_3\right)} \tag{26}$$

and

$$\theta' = \tan^{-1}\left(-\frac{\Gamma^2+1-\lambda_{\max}}{k_2\Gamma}\right) \tag{27}$$

The obtained data plot along a general path involving increasing shear strain γ and decreasing values of the stretch k_2 moving from the margin toward the shear zone centre. Using Equations 24 and 27 one can obtain the exact value of the stretch k_3 (and hence $k_2 = k_3^{-1}$) and of the shear strain γ. The finite values of the strain ratios R_{XZ}, R_{YZ} and R_{XY} and the kinematic vorticity number W_k are obtained by applying Equations 19 and 25.

In order to smooth out the data in the incremental strain analysis that will be carried out in the following

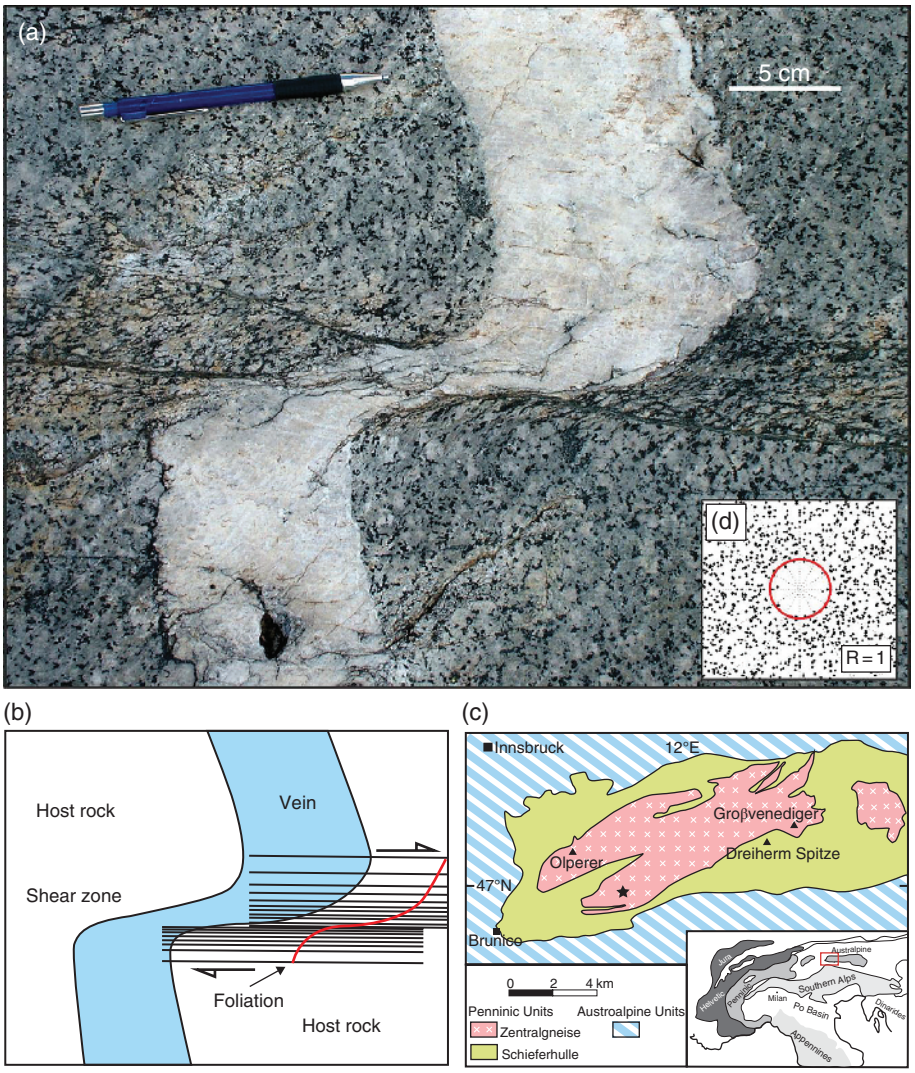

Fig. 1.3. (a) Outcrop view of the analyzed heterogeneous dextral wrench zone deforming quartz vein. (b) Subdivision into homogeneously deformed layers. (c) Geological sketch map of part of the Eastern Alps, showing site of the structural analysis (star) (modified after Pennacchioni and Mancktelow 2007). (d) Normalized Fry plot showing finite strain measured in the host rock.

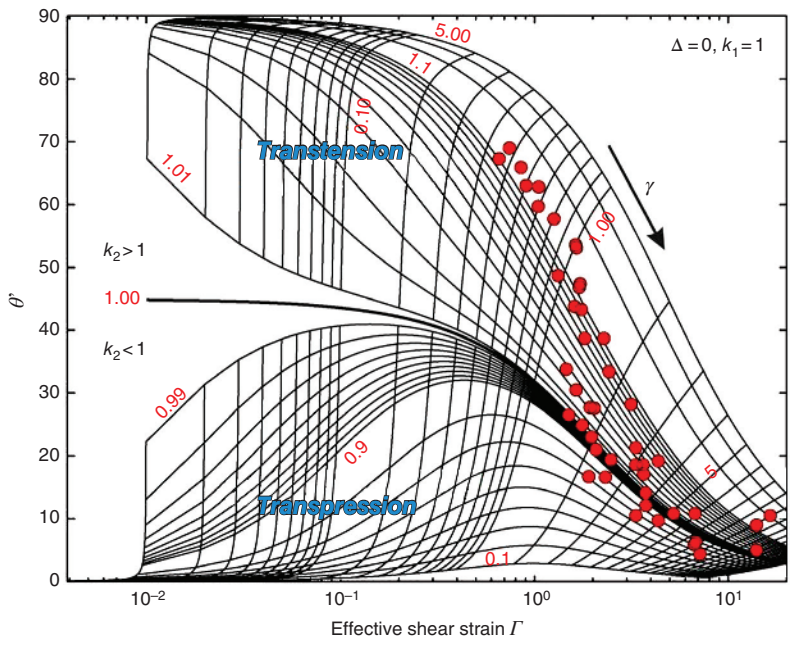

Fig. 1.4. Γ– θ' scatter diagram. The k_2–γ grid was constructed for a transpressional/transtensional deformation ($\Delta = 0$ and $k_1 = 1$).

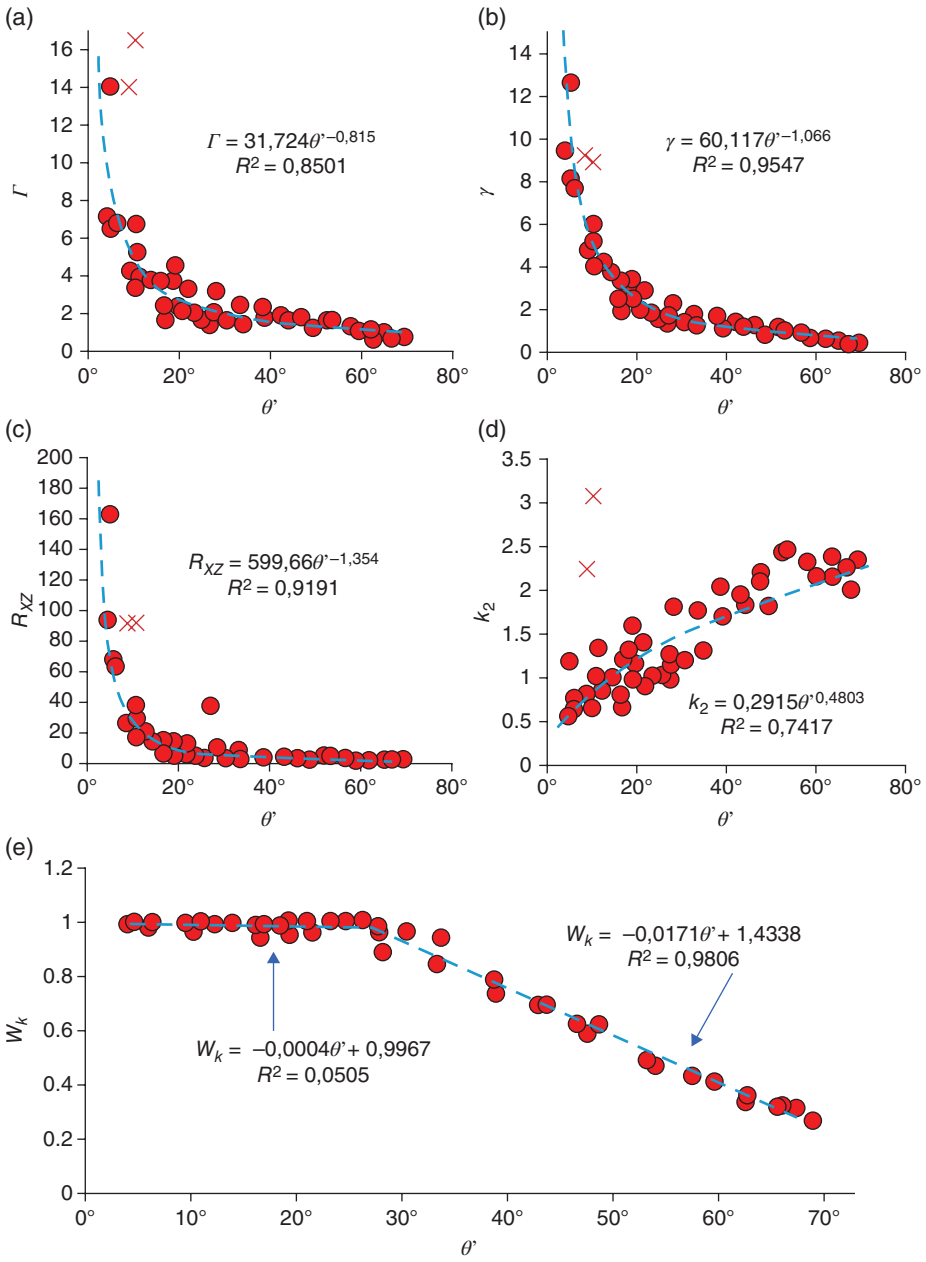

Fig. 1.5. Scatter diagrams of (a) finite effective shear strain Γ, (b) finite shear strain γ, (c) finite strain ratio R_{XZ}, (d) finite elongation k_2, and (e) finite kinematic vorticity number W_k versus finite angle θ'. Best-fit curves are also shown with associated equation and coedfficient of determination R^2.

section, best-fit power-law curves are determined for the finite values of effective shear strain Γ (Fig. 1.5a), shear strain γ (Fig. 1.5b), strain ratio R_{XZ} (Fig. 1.5c), and stretch k_2 (Fig. 1.5d) as a function of the angle θ'. A power-law curve is used to fit the scatter data because it provides the best values of the coefficient of determination R^2 (which is a measure of how well the data fit the adopted statistical model).

The finite kinematic vorticity number W_k increases linearly for θ', ranging from the maximum observed value (about 70°) to about 30°, becoming constant (and close to unity) for angles between about 30° and the minimum observed θ' values (<5°; Fig. 1.5e). Note that if the increase in effective shear strain, shear strain and strain ratio with decreasing θ' are somewhat expected, much less obvious is the decrease in elongation k_2. To evaluate finite strain in the host rock, the normalized-Fry method (Fry 1979; Erslev 1988) was applied to the rock areas surrounding the structure. The obtained values of ellipticity on the *XZ* plane (R_{XZ}^{host}) are of about 1, indicating no strain (Fig. 1.3d).

Summarizing, the ductile wrench zone is characterized by: (i) non-constant finite values of the stretches

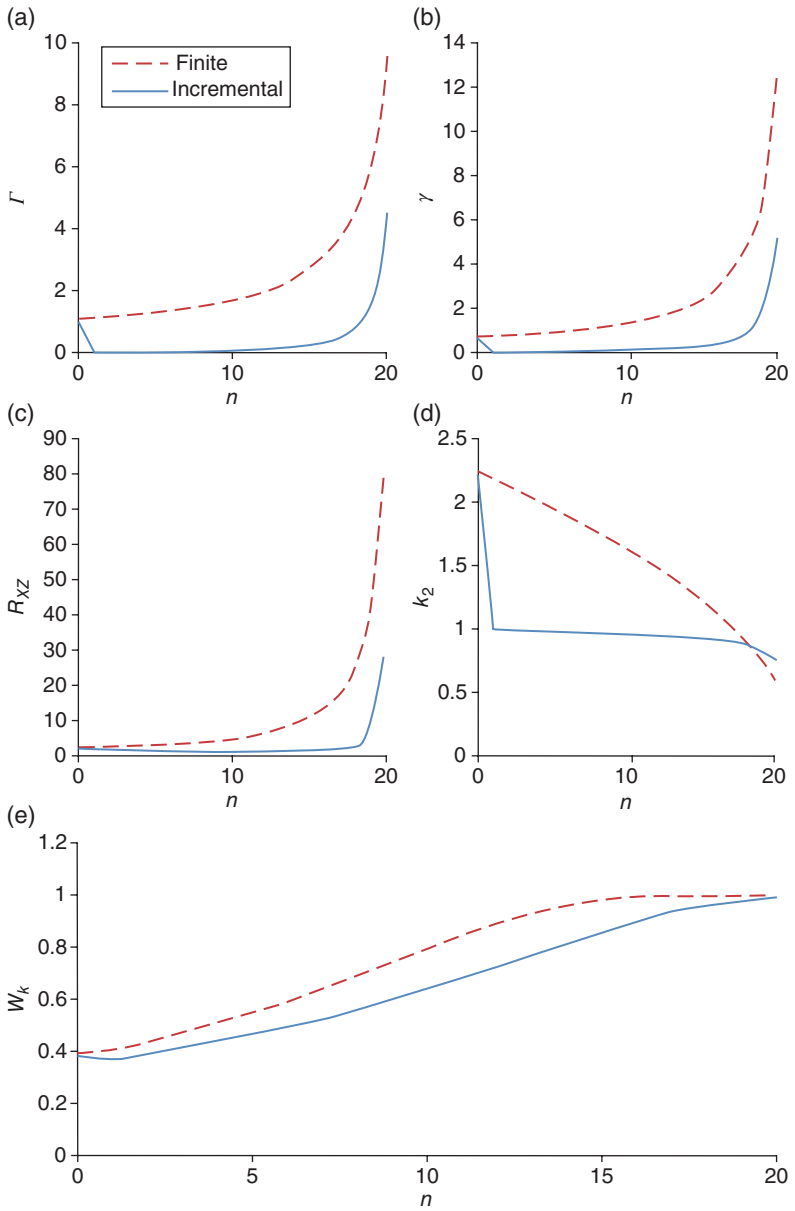

Fig. 1.6. Profiles of finite and incremental values of: (a) effective shear strain Γ, (b) shear strain γ, (c) strain ratio R_{XZ}, (d) stretch k_2, and (e) kinematic vorticity number W_k versus layer number n.

k_2 and k_3, with k_2 values mostly larger than unity (having assumed $k_1 = 1$); (ii) localized deformation occurring within the shear zone only (i.e. undeformed host rock); and (iii) no volume variation. These features point out the occurrence of material flow along the z-axis of the reference frame (i.e. in the vertical direction). This effect is dominant in the low-strain parts of the shear zone (i.e. for high values of the angle θ') characterized by k_2 values above unity (transtensional deformation), becoming negligible for the simple shear-dominated ($W_k \approx 1$) central sector of localized high strain.

1.4.2 Incremental strain

The incremental strain analysis of the studied shear zone was carried out considering a total number of $n = 20$ steps forthe application of the inverse method. For each step, discrete values of k_2 and Γ were obtained from the best-fit equations (Fig. 1.5). Equation 3 has been used to calculate the incremental strain because this shear zone displays no deformation outside of it (Fig. 1.3a, d).

Figure 1.6 displays the profiles of finite and incremental values for effective shear strain Γ, shear strain γ, stretch k_2, strain ratio R_{XZ} and kinematic vorticity number W_k versus number of steps, whereas in Fig. 1.7(a,b) finite and incremental strain paths are plotted on: (i) $\Gamma - \theta$' and (ii) logarithmic Flinn diagrams (Flinn 1962; Ramsay 1967), respectively. It must be stressed that the first incremental strain step corresponds to the first step of finite strain (transtension); on the contrary, the subsequent incremental strain values (from 2 to 20) indicate a transpressional deformation, although the finite strain is of dominantly transtensional type. For example, the first incremental value of k_2 is 2.23 (transtension), whereas

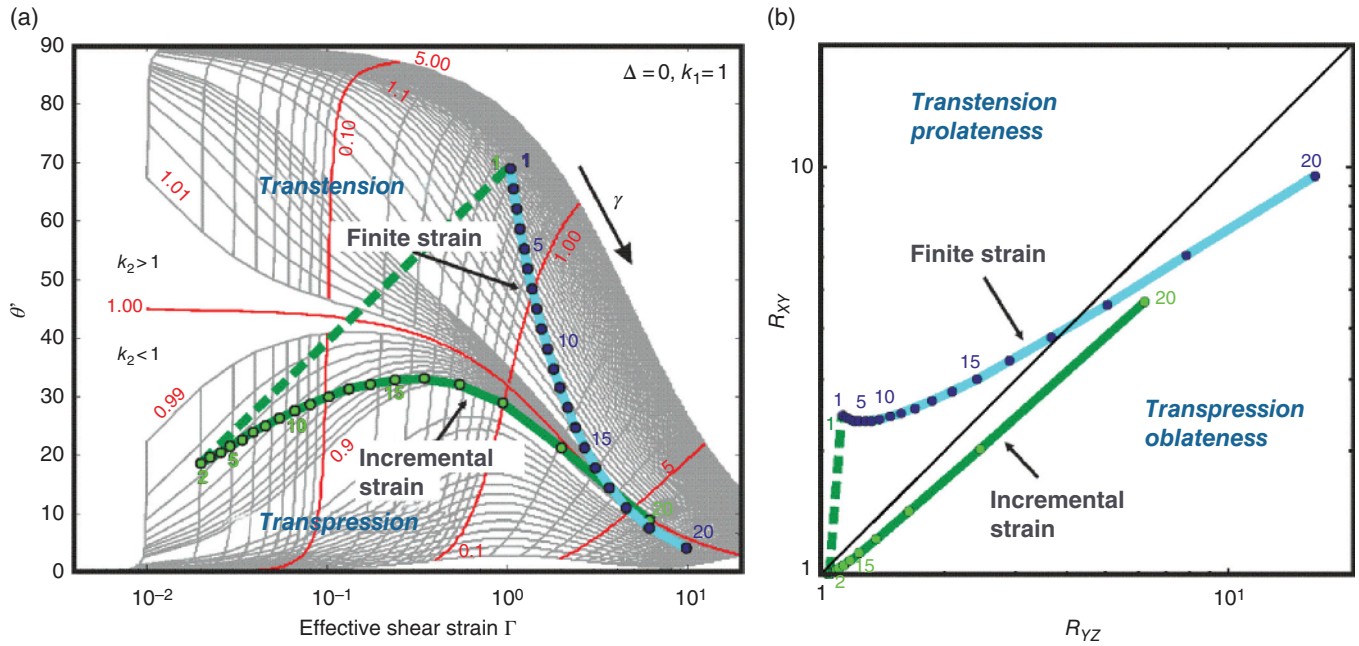

Fig. 1.7. (a) Γ– θ' and (b) logarithmic Flinn diagrams showing incremental and finite strain paths.

the following incremental k_2 path (from 2 to 20 steps, Fig. 1.7a) is generally characterized by values lower than 1, decreasing toward the center of the shear zone.

Finite and incremental profiles of effective shear strain Γ, shear strain γ and strain ratio R_{XZ} show similar peaked shapes, pointing out a non-linear increase during shear zone evolution (Fig. 1.6a–c). The peaked shape of the curve confirms the interpretation, already suggested, based on finite strain analysis, that shear zone rheology was characterized by strain softening, involving both simple shear and the pure shear components of the deformation. However, both finite and incremental kinematic vorticity numbers increase, up to unity, for increasing deformation (Fig. 1.6e). Therefore, the partitioning between simple shear and pure shear changed during shear zone evolution from prevailing pure shear ($W_k \approx 0.4$) to dominant simple shear, eventually reaching conditions of simple shear alone ($W_k \approx 1$) for the latest stages of highly localized deformation in the softened central sector of the shear zone.

The incremental strain paths plotted on the Γ– θ' diagram (Fig. 1.7a) and in the logarithmic Flinn diagram (Fig. 1.7b) confirm that the incremental strain from steps 2 to 20 consistently lies in the transpressional oblate field. Also, note that none of the incremental strain parameters holds a constant value during the temporal evolution; therefore the incremental deformation evolution is non-steady state.

As previously mentioned, the first increment points out a transtensional deformation whereas the subsequent strain increments are of transpressional type. In the case of no synchronous deformation in the host rock, the final strain configuration does not provide information about the temporal evolution of the shear zone. However, the suggested strain evolution is more consistent with a localizing shear zone (Fig. 1.1a, with **C** = 1) characterized by: (i) an early homogeneous transtensional deformation affecting the whole shear zone; and (ii) a following localization of the transpressional strain in the central part, probably driven by strain softening processes, with respect to a delocalizing shear zone (Fig. 1.1b, with **C** = 1) where an initial transtension affects the central part and subsequently migrates outward, with synchronous transpression affecting the inner sectors.

1.5 CONCLUSIONS

According to the Means hypothesis (Means 1975) and as suggested by Provost et al. (2004) and Horsman and Tikoff (2007), information on the incremental strain history may be obtained from the analysis of the final strain configuration in a heterogeneous shear zone. In particular, in case the structural evolution was characterized by strain softening or hardening – which are assumed to control the development of localizing and delocalizing shear zones, respectively – one can unravel the relationship between finite strain across the shear zone and incremental strains. Based on this assumption, an inverse method was derived which is able to evaluate the incremental strain matrices starting from measured finite strain quantities in a heterogeneous ductile shear zone. The proposed technique uses the finite values of the effective shear strain Γ and the finite angle θ' (angle between the foliation, i.e. the *xy* plane of the finite strain ellipsoid, and the shear plane) obtained for *n* layers, in

which a shear zone may be subdivided according to homogeneity criteria. Shear zone deformation may then be described in terms of *n* finite strain matrices, each representing homogeneous deformation of the related layer. Starting from these matrices, it is possible to derive the incremental strain matrices. For simple cases, the proposed method furnishes symbolic formulae relating finite and incremental values of the main strain parameters, such as shear strain and stretches. The inverse method requires knowing the strain parameters k_1, k_2, k_3, and Γ. In particular instances such as that analyzed in this paper, it is possible to derive all of the required strain parameters from simple formulae. For the analyzed wrench zone, characterized by no stretches along the *x* direction and no volume change, the incremental strain path suggests a localizing shear zone evolution characterized by an initial homogeneous transtensional deformation in the whole shear zone and a subsequent incremental transpression driven by strain softening processes affecting progressively inner sectors.

ACKNOWLEDGMENTS

We thank Soumyajit Mukherjee for editorial assistance and useful suggestions and the two anonymous reviewers for the precious comments and corrections. Thanks to Kelvin Matthews, Delia Sandford, and Ian Francis (Wiley Blackwell) for support.

REFERENCES

Alsleben H, Wetmore PH, Schmidt KL, Paterson SR. 2008. Complex deformation as a result of arc-continent collision: Quantifying finite strain in the Alisitos arc, Peninsular Ranges, Baja California. Journal of Structural Geology 30, 220–236.

Dasgupta N, Mukhopadhyay D, Bhattacharyya T. 2012. Analysis of superposed strain: A case study from Barr Conglomerate in the South Delhi Fold Belt, Rajasthan, India. Journal of Structural Geology 34, 30–42.

Davis JR, Titus SJ. 2011. Homogeneous steady deformation: A review of computational techniques. Journal of Structural Geology 33, 1046–1062.

Dunnet D. 1969. A technique of finite strain analysis using elliptical particles. Tectonophysics 7, 117–136.

Erslev EA. 1988. Normalized center-to-center strain analysis of packed aggregates. Journal of Structural Geology 10, 201–209.

Flinn D. 1962. On folding during three-dimensional progressive deformation. Quarterly Journal of the Geological Society of London 118, 385–428.

Fossen H, Tikoff B. 1993. The deformation matrix for simultaneous simple shearing, pure shearing and volume change, and its application to transpression–transtension tectonics. Journal of Structural Geology 15, 413–422.

Fry N. 1979. Random point distributions and strain measurement in rocks. Tectonophysics 60, 89–105.

Grant JA. 1986. The isocon diagram – a simple solution to Gresens' equation for metasomatic alteration. Economic Geology 81, 1976–1982.

Horsman E, Tikoff B. 2007.Constraints on deformation path from finite strain gradients. Journal of Structural Geology 29, 256–272.

Hull J. 1988. Thickness-displacement relationships for deformation zones. Journal of Structural Geology 10, 431–435.

Iannace A, Vitale S. 2004. Ductile shear zones on carbonates: the *calcaires plaquettés* of Northern Calabria (Italy). Comptes Rendues Geosciences 336, 227–234.

Kuiper YD, Lin S, Jiang D. 2011. Deformation partitioning in transpressional shear zones with an along-strike stretch component: An example from the Superior Boundary Zone, Manitoba, Canada. Journal of Structural Geology 33, 192–202.

Lisle RJ. 1985. Geological Strain Analysis: A Manual for the Rf/ϕ Method. Pergamon Press, Oxford.

Mancktelow NS, Pennacchioni G. 2005. The control of precursor brittle fracture and fluid-rock interaction on the development of single and paired ductile shear zones. Journal of Structural Geology 27, 645–661.

Mazzoli S, Di Bucci D. 2003. Critical displacement for normal fault nucleation from en-échelon vein arrays in limestones: a case study from the southern Apennines (Italy). Journal of Structural Geology 25, 1011–1020.

Mazzoli S, Invernizzi C, Marchegiani L, Mattioni L, Cello G. 2004. Brittle-ductile shear zone evolution and fault initiation in limestones, Monte Cugnone (Lucania), southern Apennines, Italy. In Transport and Flow Processes in Shear Zones, edited by I. Alsop, and R.E. Holdsworth, Geological Society, London, Special Publications, 224, pp. 353–373.

Mazzoli S, Vitale S, Delmonaco G, Guerriero V, Margottini C, Spizzichino D, 2009. "Diffuse faulting" in the Machu Picchu granitoid pluton, Eastern Cordillera, Peru. Journal of Structural Geology 31, 1395–1408.

Means WD. 1995. Shear zones and rock history. Tectonophysics 247, 157–160.

Mitra G. 1991. Deformation of granitic basement rocks along fault zones at shallow to intermediate crustal levels. In Structural Geology of Fold and Thrust Belts, edited by S. Mitra, and G. W. Fisher, Johns Hopkins University Press, Baltimore, pp. 123–144.

Mukherjee S. 2013. Deformation Microstructures in Rocks. Springer, Heidelberg.

Mukherjee S. 2014. Atlas of shear zone structures in Meso-scale. Springer International Publishing, Cham.

Okudaira T, Beppu Y. 2008. Inhomogeneous deformation of metamorphic tectonites of contrasting lithologies: Strain analysis of metapelite and metachert from the Ryoke metamorphic belt, SW Japan. Journal of Structural Geology 30, 39–49.

Passchier C, Trouw R. 2005. Microtectonics. Springer Verlag, Berlin.

Provost A, Buisson C, Merle O. 2004. From progressive to finite deformation and back. Journal of Geophysical Research: Solid Earth and Planets 109, B02405.

Pennacchioni G. 2005. Control of the geometry of precursor brittle structures on the type of ductile shear zone in the Adamello tonalites, Southern Alps (Italy). Journal of Structural Geology 27, 627–644.

Pennacchioni G, Mancktelow NS. 2007. Nucleation and initial growth of a shear zone network within compositionally and structurally heterogeneous granitoids under amphibolite facies conditions. Journal of Structural Geology 29, 1757–1780.

Ramsay JG. 1967. Folding and Fracturing of Rocks. McGraw-Hill, New York.

Ramsay JG. 1980. Shear zone geometry: a review. Journal of Structural Geology 2, 83–99.

Ramsay JG, Huber M. 1983. The Techniques of Modern Structural Geology. Volume I: Strain Analysis, Academic Press, London.

Samani B. 2013. Quartz c-axis evidence for deformation characteristics in the Sanandaj–Sirjan metamorphic belt, Iran. Journal of African Earth Sciences 81, 28–34.

Sanderson D, Marchini RD. 1984. Transpression. Journal of Structural Geology 6, 449–458.

Sarkarinejad K, Samani B, Faghih A, Grasemann B, Moradipoor M. 2010. Implications of strain and vorticity of flow analyses to interpret the kinematics of an oblique convergence event (Zagros Mountains, Iran). Journal of Asian Earth Sciences 38, 34–43.

Tikoff B, Fossen H. 1993. Simultaneous pure and simple shear: the unified deformation matrix. Tectonophysics 217, 267–283.

Vitale S, Mazzoli S. 2005. Influence of object concentration on finite strain and effective viscosity contrast: Insights from naturally deformed packstones. Journal of Structural Geology 27, 2135–2149.

Vitale S, Mazzoli S. 2008. Heterogeneous shear zone evolution: the role of shear strain hardening/softening. Journal of Structural Geology 30, 1363–1395.

Vitale S, Mazzoli S. 2009. Finite strain analysis of a natural ductile shear zone in limestones: insights into 3-D coaxial vs. non-coaxial deformation partitioning. Journal of Structural Geology 31, 104–113.

Vitale S, Mazzoli S. 2010. Strain analysis of heterogeneous ductile shear zones based on the attitude of planar markers. Journal of Structural Geology 32, 321–329.

Vitale S, Iannace A, Mazzoli S. 2007a. Strain variations within a major carbonate thrust sheet of the Apennine collisional belt, northern Calabria, southern Italy. In Deformation of the Continental Crust: The Legacy of Mike Coward, edited by A.C. Ries, R.W.H. Butler, and R.H. Graham, Geological Society, London, Special Publications 272, pp. 145–156.

Vitale S, White JC, Iannace A, Mazzoli S. 2007b. Ductile strain partitioning in micritic limestones, Calabria, Italy: the roles and mechanisms of intracrystalline and intercrystalline deformation. Canadian Journal of Earth Sciences 44, 1587–1602.

Yonkee A. 2005. Strain patterns within part of the Willard thrust sheet, Idaho–Utah–Wyoming thrust belt. Journal of Structural Geology 27, 1315–1343.

Zhang Q, Giorgis S, Teyssier C. 2013. Finite strain analysis of the Zhangbaling metamorphic belt, SE China e Crustal thinning in transpression. Journal of Structural Geology 49, 13–22.